



CERN-EP-2017-289
 LHCb-PAPER-2017-032
 November 15, 2017

First observation of $B^+ \rightarrow D_s^+ K^+ K^-$ decays and a search for $B^+ \rightarrow D_s^+ \phi$ decays

The LHCb collaboration[†]

Abstract

A search for $B^+ \rightarrow D_s^+ K^+ K^-$ decays is performed using pp collision data corresponding to an integrated luminosity of 4.8 fb^{-1} , collected at centre-of-mass energies of 7, 8 and 13 TeV with the LHCb experiment. A significant signal is observed for the first time and the branching fraction is determined to be

$$\mathcal{B}(B^+ \rightarrow D_s^+ K^+ K^-) = (7.1 \pm 0.5 \pm 0.6 \pm 0.7) \times 10^{-6},$$

where the first uncertainty is statistical, the second systematic and the third due to the uncertainty on the branching fraction of the normalisation mode $B^+ \rightarrow D_s^+ \bar{D}^0$. A search is also performed for the pure annihilation decay $B^+ \rightarrow D_s^+ \phi$. No significant signal is observed and a limit of

$$\mathcal{B}(B^+ \rightarrow D_s^+ \phi) < 4.9 \times 10^{-7} \quad (4.2 \times 10^{-7})$$

is set on the branching fraction at 95% (90%) confidence level.

Published in JHEP 01 (2018) 131

© CERN on behalf of the LHCb collaboration, licence CC-BY-4.0.

[†]Authors are listed at the end of this paper.

1 Introduction

The decay $B^+ \rightarrow D_s^+ K^+ K^-$ is mediated by a $\bar{b} \rightarrow \bar{u}$ transition shown in Fig. 1 and is therefore suppressed in the Standard Model (SM) due to the small size of the Cabibbo-Kobayashi-Maskawa (CKM) matrix element V_{ub} . The branching fraction for this decay is currently not measured, however a similar decay, $B^+ \rightarrow D_s^+ \pi^0$, has been observed with a branching fraction of $\mathcal{B}(B^+ \rightarrow D_s^+ \pi^0) = (1.5 \pm 0.5) \times 10^{-5}$ [1].

In the SM, the decay $B^+ \rightarrow D_s^+ \phi$ proceeds dominantly via the annihilation diagram shown in Fig. 1. This suppressed topology requires the wave functions of the incoming quarks to overlap sufficiently to annihilate into a virtual W^+ boson. The decay is further suppressed by the small magnitude of the CKM matrix element V_{ub} associated with the annihilation vertex. In addition, unlike many rare hadronic decays including $B^+ \rightarrow D_s^+ K^+ K^-$, possible contributions from rescattering effects are expected to be small, for example contributions from intermediate states such as $B^+ \rightarrow D_s^+ \omega$ [2]. Several SM predictions have been made for the branching fraction of the $B^+ \rightarrow D_s^+ \phi$ decay [3–6], using input from lattice calculations [7–9]. These predictions are in the range $(1–7) \times 10^{-7}$, where the limit on the precision is dominated by hadronic uncertainties. However, additional diagrams contributing to this decay can arise in some extensions of the SM, such as supersymmetric models with R-parity violation. They could enhance the branching fraction and/or produce large CP asymmetries [4, 5], which makes the $B^+ \rightarrow D_s^+ \phi$ decay a promising place to search for new physics beyond the SM.¹

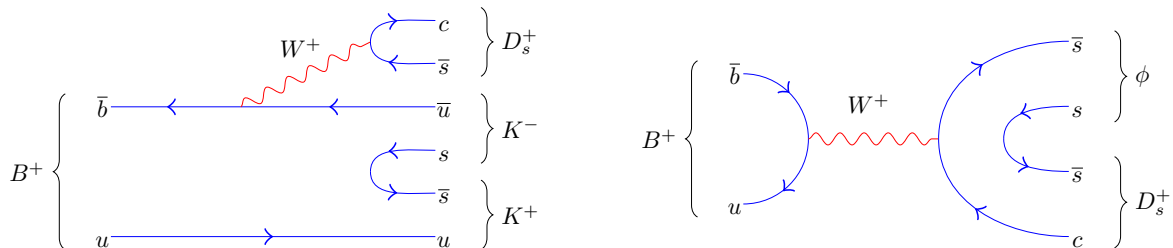


Figure 1: Dominant diagram for the (left) $B^+ \rightarrow D_s^+ K^+ K^-$ decay and (right) annihilation diagram for the $B^+ \rightarrow D_s^+ \phi$ decay in the Standard Model.

The LHCb experiment reported evidence for the decay $B^+ \rightarrow D_s^+ \phi$ using pp collision data corresponding to an integrated luminosity of 1 fb^{-1} taken during 2011, at a centre-of-mass energy of 7 TeV [10]. A total of $6.7_{-2.6}^{+4.5}$ candidates was observed. The branching fraction was determined to be

$$\mathcal{B}(B^+ \rightarrow D_s^+ \phi) = (1.87_{-0.73}^{+1.25} \pm 0.19 \pm 0.32) \times 10^{-6}, \quad (1)$$

where the first uncertainty is statistical, the second is systematic and the third is due to the uncertainty on the branching fraction of the decay $B^+ \rightarrow D_s^+ \bar{D}^0$, which was used as normalisation. Given the large uncertainties on both the theoretical and experimental values, the previously measured value is consistent with the range of SM values given above. The measurements presented in this paper reanalyse the data collected in 2011, whilst adding data corresponding to an integrated luminosity of 2 fb^{-1} collected at a centre-of-mass energy 8 TeV in 2012, along with 0.3 fb^{-1} from 2015 and 1.5 fb^{-1} from 2016, both at 13 TeV. They supersede the previous measurement [10].

¹Charge conjugation is implied throughout this paper. Furthermore, ϕ denotes the $\phi(1020)$ resonance.

This analysis is performed in two parts: firstly $B^+ \rightarrow D_s^+ K^+ K^-$ decays are reconstructed across the entire phase space and then a dedicated search for $B^+ \rightarrow D_s^+ \phi$ decays is performed in a narrow region of $K^+ K^-$ invariant mass around the ϕ meson. The branching fractions are determined using the decay $B^+ \rightarrow D_s^+ \bar{D}^0$, with $\bar{D}^0 \rightarrow K^+ K^-$, as a normalisation channel. Although this \bar{D}^0 decay has a smaller branching fraction than $\bar{D}^0 \rightarrow K^+ \pi^-$ (0.4% vs. 3.9% [11]), sharing the same final state between the signal and normalisation channel reduces systematic uncertainties in the ratio of detection efficiencies.

2 Detector and data sample

The LHCb detector [12, 13] is a single-arm forward spectrometer covering the pseudorapidity range $2 < \eta < 5$, designed for the study of particles containing b or c quarks. The detector includes a high-precision tracking system consisting of a silicon-strip vertex detector surrounding the pp interaction region, a large-area silicon-strip detector located upstream of a dipole magnet with a bending power of about 4 Tm, and three stations of silicon-strip detectors and straw drift tubes placed downstream of the magnet. The tracking system provides a measurement of momentum, p , of charged particles with a relative uncertainty that varies from 0.5% at low momentum to 1.0% at 200 GeV/ c . The minimum distance of a track to a primary pp interaction vertex (PV), the impact parameter (IP), is measured with a resolution of $(15 + 29/p_T) \mu\text{m}$, where p_T is the component of the momentum transverse to the beam, in GeV/ c . Different types of charged hadrons are distinguished using information from two ring-imaging Cherenkov detectors. Photons, electrons and hadrons are identified by a calorimeter system consisting of scintillating-pad and preshower detectors, an electromagnetic calorimeter and a hadronic calorimeter. Muons are identified by a system composed of alternating layers of iron and multiwire proportional chambers. The online event selection is performed by a trigger, which consists of a hardware stage, based on information from the calorimeter and muon systems, followed by a software stage, which applies a full event reconstruction.

At the hardware trigger stage, events are required to have a muon with high p_T or a hadron, photon or electron with high transverse energy in the calorimeters. Two different algorithms are used in the software trigger to select candidates for this analysis. The first uses a multivariate algorithm [14] to identify the presence of a secondary vertex that has two, three or four tracks and is displaced from any PV. At least one of these charged particles must have a transverse momentum $p_T > 1.7 \text{ GeV}/c$ and be inconsistent with originating from a PV. The second algorithm selects ϕ candidates decaying to two charged kaons. Each kaon must have a transverse momentum $p_T > 0.8 \text{ GeV}/c$ and be inconsistent with originating from a PV. The invariant mass of the kaon pair must be within $20 \text{ MeV}/c^2$ of the known ϕ mass [11]. This algorithm is used in both the search for $B^+ \rightarrow D_s^+ \phi$ and $B^+ \rightarrow D_s^+ K^+ K^-$ decays.

Simulated events are used to determine the relative efficiencies of the signal and normalisation channels. The samples are generated for each of the running periods. In these simulations, pp collisions are generated using PYTHIA [15, 16] with a specific LHCb configuration [17]. Decays of hadronic particles are described by EVTGEN [18], in which final-state radiation is generated using PHOTOS [19]. The interaction of the generated particles with the detector, and its response, are implemented using the GEANT4

toolkit [20] as described in Ref. [21].

3 Candidate selection

Candidate $B^+ \rightarrow D_s^+ \phi$ and $B^+ \rightarrow D_s^+ K^+ K^-$ decays are selected using similar requirements. The ϕ mesons in $B^+ \rightarrow D_s^+ \phi$ candidates are reconstructed with $\phi \rightarrow K^+ K^-$. Both modes are reconstructed using the $D_s^+ \rightarrow K^+ K^- \pi^+$ decay, whilst $B^+ \rightarrow D_s^+ \phi$ candidates are additionally reconstructed with the decays $D_s^+ \rightarrow K^+ \pi^- \pi^+$ and $D_s^+ \rightarrow \pi^+ \pi^- \pi^+$ to increase the sensitivity of the search. The D_s^+ (ϕ) candidates are required to have an invariant mass within $25 \text{ MeV}/c^2$ ($40 \text{ MeV}/c^2$) of the known D_s^+ (ϕ) mass [11]. In the search for $B^+ \rightarrow D_s^+ K^+ K^-$ decays, the veto $|m(K^+ K^-) - m(D^0)| > 25 \text{ MeV}/c^2$ is applied to explicitly remove the normalisation channel from the signal mode.

The B^+ meson candidates are formed from well reconstructed tracks with $\chi_{\text{IP}}^2 > 4.0$, where χ_{IP}^2 is defined as the difference in the vertex-fit χ^2 of the best PV reconstructed with and without the particle being considered. The best PV is the PV that has the smallest χ_{IP}^2 value. For kaons from the ϕ or B^+ decay the momentum requirement is $p > 2 \text{ GeV}/c$. At least one track of each B^+ meson candidate must have $p_{\text{T}} > 0.5 \text{ GeV}/c$ and $p > 5 \text{ GeV}/c$.

Loose requirements are made on particle identification (PID) to reduce background from other b -hadron decays with misidentified hadrons. For the signal, the overall efficiency of the PID requirements varies from 80% to 90%, depending on the D_s^+ mode. Background from decays of B^+ mesons to the same final state that did not proceed via a D_s^+ meson (referred to as charmless decays) are suppressed by applying a requirement on the significance of the B^+ and D_s^+ vertex separation, χ_{FD}^2 .

The residual yields of charmless decays are estimated by determining the B^+ yield in candidates that are in the invariant mass range $25 < |m(h^+ h'^- \pi^+) - m(D_s^+)| < 50 \text{ MeV}/c^2$, where $m(h^+ h'^- \pi^+)$ is the D_s^+ candidate mass and $h, h' = K, \pi$. This background estimation is performed separately for the $B^+ \rightarrow D_s^+ \phi$ and $B^+ \rightarrow D_s^+ K^+ K^-$ searches. For the $B^+ \rightarrow D_s^+ \bar{D}^0$ normalisation channel, a two-dimensional optimisation is performed to calculate the contribution from decays without a D_s^+ meson, \bar{D}^0 meson or both. The optimal selection requirements are chosen such that the maximum signal efficiency is achieved for a residual charmless contribution of 2% of the normalisation yield.

For the decay $D_s^+ \rightarrow K^+ K^- \pi^+$, candidates are rejected if they are consistent with $D^+ \rightarrow K^- \pi^+ \pi^+$ or $\Lambda_c^+ \rightarrow p K^- \pi^+$ decays, where either a pion or a proton has been misidentified as a kaon. The candidates are reconstructed using the alternative mass hypothesis and, for those falling within $25 \text{ MeV}/c^2$ of the D^+ or Λ_c^+ mass, particle identification requirements are tightened on the misidentified track.

Another set of vetoes rejects decays where the tracks forming the D_s^+ candidate originate from an excited charged charm meson decay, for example $D^{*+} \rightarrow (D^0 \rightarrow h^+ h'^-) \pi^+$. By requiring $\Delta m = m(h^+ h'^- \pi^+) - m(h^+ h'^-) > 150 \text{ MeV}/c^2$ decays of this type are efficiently removed. Other specific backgrounds are removed by mass vetoes. These vetoes remove $B_s^0 \rightarrow \phi \phi$ decays in which one of the ϕ mesons is combined with an unrelated pion to form the D_s^+ candidate. Any candidates within $50 \text{ MeV}/c^2$ of the known B_s^0 mass [11] in the four-body invariant mass $m(K^+ K^- K^+ K^-)$ are removed to ensure a smooth combinatorial background distribution.

In addition, a veto is applied to the invariant mass of the kaons from the ϕ meson

or B^+ candidate combined with any pion from the D_s^+ candidate, removing candidates within $25 \text{ MeV}/c^2$ of the known D_s^+ mass. This removes decays that include incorrectly reconstructed $D_s^+ \rightarrow \phi\pi^+$ or $D_s^+ \rightarrow K^+K^-\pi^+$ decays, where the ϕ or K^+K^- pair are incorrectly assigned to have originated from the B^+ meson rather than the D_s^+ meson. For example, this incorrect assignment could lead to $B^+ \rightarrow (D_s^+ \rightarrow \phi\pi^+)K^+K^-$ decays being reconstructed as $B^+ \rightarrow (D_s^+ \rightarrow K^+K^-\pi^+)\phi$ decays. The B^+ (D_s^+) candidates are required to have $\chi_{\text{IP}}^2 < 10$ ($\chi_{\text{IP}}^2 > 10$), to ensure they are consistent (inconsistent) with being produced at the best PV.

Multivariate analyses (MVA) are used to separate genuine ϕ and D_s^+ candidates from random combinations of tracks [22]. The ϕ and D_s^+ MVAs use data samples of $B_s^0 \rightarrow J/\psi\phi$ and $\bar{B}_s^0 \rightarrow D_s^+\pi^-$ decays, respectively, where the background is statistically subtracted using the *sPlot* method [23]. The training uses the ϕ or D_s^+ sidebands as a background sample. A total of eight MVAs are trained to target the decays $\phi \rightarrow K^+K^-$, $D_s^+ \rightarrow K^+K^-\pi^+$, $D_s^+ \rightarrow K^+\pi^-\pi^+$ and $D_s^+ \rightarrow \pi^+\pi^-\pi^+$, separately in the Run 1 (2011 and 2012) and Run 2 (2015 and 2016) data. A preselection including the trigger, vetoes and PID requirements previously discussed is applied to the training samples, ensuring they are representative of the target signal decays. The samples are split into two subsamples in a random but reproducible way. One is used to train the corresponding MVA, the other to test its response.

The MVA method used in this analysis is a gradient Boosted Decision Tree (BDTG) [24]. The selection criteria for each of the BDTG classifiers are determined by optimising the figure of merit $\epsilon_s/(\frac{a}{2} + \sqrt{N_{\text{BKG}}})$ [25], with $a = 5$, where ϵ_s is the signal efficiency and N_{BKG} is the number of background candidates determined from fits to data, calculated in the signal region.

The efficiencies of the MVAs are obtained from the test samples of $B_s^0 \rightarrow J/\psi\phi$ and $\bar{B}_s^0 \rightarrow D_s^+\pi^-$ decays. Additionally, a sample of $B^+ \rightarrow \bar{D}^0\pi^+$ decays is used to calculate the efficiency of $\bar{D}^0 \rightarrow K^+K^-$ decays in the normalisation channel. The efficiency calculation takes into account the kinematic differences between the training and signal samples, as well as any possible correlations between the D_s^+ and ϕ kinematics, by using input from simulation samples. Any further correlations between the ϕ and D_s^+ MVA efficiencies are found to be negligible. In the search for $B^+ \rightarrow D_s^+K^+K^-$ decays, calibration samples are used to correct for the imperfect modelling of the PID in simulation. These corrected samples are then used to obtain the variations in the MVA efficiencies as a function of the phase-space position, in particular of the $m(K^+K^-)$ invariant mass.

The invariant mass of the B^+ meson candidates is determined from fits in which the D_s^+ candidate mass (and \bar{D}^0 candidate mass for the normalisation channel) is constrained to the known value [26]. Additionally, the momentum vector of the B^+ meson is constrained to be parallel to the vector connecting the PV and the B^+ meson decay vertex.

4 Invariant mass fits

The branching fractions of the $B^+ \rightarrow D_s^+\phi$ and $B^+ \rightarrow D_s^+K^+K^-$ decays are determined from unbinned maximum likelihood fits to the invariant mass of the B^+ candidates. However, separate fit strategies are used for the $B^+ \rightarrow D_s^+\phi$ and $B^+ \rightarrow D_s^+K^+K^-$ searches.

The search for $B^+ \rightarrow D_s^+K^+K^-$ involves two independent fits for the signal and

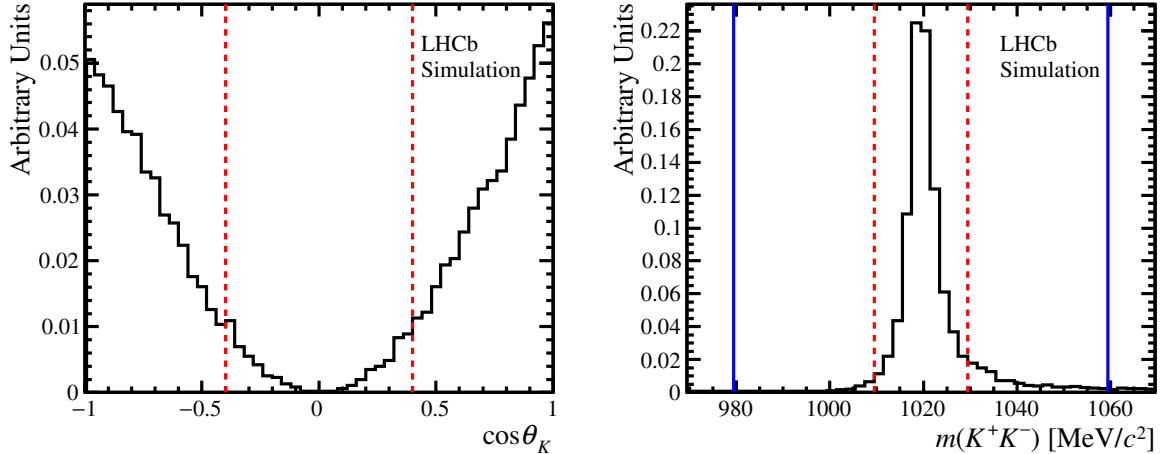


Figure 2: Distributions of (left) $\cos\theta_K$ and (right) $m(K^+K^-)$ in $B^+ \rightarrow D_s^+\phi$ decays, as determined from simulated events. The vertical lines represent the limits of the two categories used for each variable. In the $m(K^+K^-)$ distribution, the area within the dashed red lines represents the ϕ signal region, and the two areas between the dashed red and blue lines represent the ϕ sideband region. The $B^+ \rightarrow D_s^+\phi$ signal decays are seen to primarily contribute to the ϕ signal region and the $|\cos\theta_K| > 0.4$ category.

normalisation channels. The $B^+ \rightarrow D_s^+K^+K^-$ yield is corrected on a per-candidate basis to account for the phase-space dependence of the signal efficiencies in this three-body decay.

In contrast, the $B^+ \rightarrow D_s^+\phi$ candidates are treated as quasi-two-body decays in which all signal candidates are corrected with the same efficiency. The $B^+ \rightarrow D_s^+\phi$ signal and normalisation channels are fitted simultaneously in different categories, as are the three D_s^+ decay modes, with the $D_s^+ \rightarrow K^+K^-\pi^+$ mode split further into $D_s^+ \rightarrow \phi\pi^+$ and non- ϕ submodes. This exploits the high purity of the $D_s^+ \rightarrow \phi\pi^+$ decay. As the $B^+ \rightarrow D_s^+\phi$ decay involves the decay of a pseudoscalar particle to a pseudoscalar and vector particle, the ϕ vector meson ($J^P = 1^-$) must be produced longitudinally polarised. For a longitudinally polarised ϕ meson decaying to K^+K^- , the distribution of the angle θ_K , defined as the angle that the kaon meson forms with the B momentum in the ϕ rest frame, is proportional to $\cos^2\theta_K$. The distribution of $\cos\theta_K$ for $B^+ \rightarrow D_s^+\phi$ as determined from simulated events is shown in Fig. 2. In the simultaneous fit for $B^+ \rightarrow D_s^+\phi$ candidates the candidates are split into two helicity categories: $|\cos\theta_K| > 0.4$ and $|\cos\theta_K| < 0.4$. In simulated events, 93% of $B^+ \rightarrow D_s^+\phi$ decays are found in the first category, whereas for the normalisation decay and background modes, as the distributions in $\cos\theta_K$ are approximately flat, only 60% of candidates fall into this category. Additionally, the fit further assigns candidates into two $m(K^+K^-)$ invariant mass categories, $|m(K^+K^-) - m_\phi| < 10 \text{ MeV}/c^2$ and $10 < |m(K^+K^-) - m_\phi| < 40 \text{ MeV}/c^2$ (Fig. 2), to help constrain the contribution from the different backgrounds in the signal region. Background modes involving two kaons that did not originate from a ϕ meson (for example $\bar{B}_s^0 \rightarrow D_s^{(*)+}K^-K^{*0}$) have different fractions in these two categories, helping to distinguish them from those decays with a real ϕ meson. The fractions of $B^+ \rightarrow D_s^+\phi$ candidates in each of the categories, as determined from simulated events, are listed in Table 1.

Table 1: Fractions of $B^+ \rightarrow D_s^+ \phi$ candidates expected in the helicity and $m(K^+K^-)$ invariant mass categories of the simultaneous fit.

$ m(K^+K^-) - m_\phi $ (MeV/ c^2)	Helicity Category	
	$ \cos \theta_K > 0.4$	$ \cos \theta_K < 0.4$
< 10	82%	6%
(10, 40)	11%	1%

Table 2: Fractions of $B^+ \rightarrow D_s^+ K^+ K^-$ candidates assumed to contribute to each helicity and $m(K^+K^-)$ invariant mass categories of the simultaneous fit. The uncertainties shown are calculated from the range of fractions obtained by assuming different contributing resonances, as detailed in Sec. 4.1.

$ m(K^+K^-) - m_\phi $ (MeV/ c^2)	Helicity Category	
	$ \cos \theta_K > 0.4$	$ \cos \theta_K < 0.4$
< 10	$(15 \pm 2)\%$	$(10 \pm 1)\%$
(10, 40)	$(45 \pm 2)\%$	$(30 \pm 1)\%$

4.1 Signal and normalisation probability density functions

The normalisation and signal components in the $B^+ \rightarrow D_s^+ \bar{D}^0$ and $B^+ \rightarrow D_s^+ K^+ K^-$ or $B^+ \rightarrow D_s^+ \phi$ invariant mass distributions are each modelled using the sum of two Crystal Ball (CB) [27] probability density functions (PDFs) with tails at lower invariant mass. The tail parameters, the ratio of the two CB widths, and the relative fraction of each CB function are determined from simulated events. The resolution parameter of the narrow CB component in each D_s^+ decay mode category is a free parameter in the fit, but the ratios of signal and normalisation widths are fixed to values determined from simulated events. For the normalisation mode, the fraction of $B^+ \rightarrow D_s^+ \bar{D}^0$ candidates in the two helicity bins is a free parameter in the fit, whereas for the signal the fraction in each helicity and $m(K^+K^-)$ invariant mass category of the fit is fixed to that determined from simulated events, as reported in Table 1.

The search for $B^+ \rightarrow D_s^+ \phi$ decays includes a component for $B^+ \rightarrow D_s^+ K^+ K^-$ decays that did not proceed via a ϕ meson. The fraction of $B^+ \rightarrow D_s^+ K^+ K^-$ decays expected in each helicity angle and $m(K^+K^-)$ mass category, shown in Table 2, are calculated from the average of different K^+K^- resonances that could contribute to $B^+ \rightarrow D_s^+ K^+ K^-$ decays. These resonances include possible contributions from the $f_0(980)$ and $a_0(980)$ resonances. The resulting fractions are sufficiently different from those for the $B^+ \rightarrow D_s^+ \phi$ signal such that the two contributions can be distinguished. The range of fractions obtained by considering the different resonances are included as uncertainties in Table 2. A systematic uncertainty is assigned to account for the fixed fractions assumed in the fit. No attempt is made to separate any of the contributing resonances in the search for $B^+ \rightarrow D_s^+ K^+ K^-$ candidates.

4.2 Background PDFs

A number of background components are included in the fit model. The dominant source of background under the signal is due to combinations of unrelated tracks. An exponential function is used to parametrise this component. The same slope parameter is used in the simultaneous fit to the signal and normalisation modes. Partially reconstructed $B^+ \rightarrow D_s^{*+} \bar{D}^0$ and $B^+ \rightarrow D_s^+ \bar{D}^{*0}$ decays are concentrated in the lower part of the $D_s^+ \bar{D}^0$ spectrum. They are parametrised using analytical shapes that account for the nonreconstructed neutral pion or photon from the excited D -meson decays. These shapes are constructed from Gaussian distributions convolved with second-order polynomials, and are analogous to those used in similar analyses [28]. An additional component is used to model $B^+ \rightarrow D_s^{*+} \bar{D}^{*0}$ decays where one particle from each of the excited D mesons is missed. Partially reconstructed $B^+ \rightarrow D_s^{*+} \phi$ decays can contribute to the lower part of the $D_s^+ \phi$ spectrum. These, similarly, are fitted with analytical shapes that account for the missing neutral particle from the D_s^{*+} decay, as well as the different helicity states for the decay of a pseudoscalar meson to two vector particles. They are parametrised in an analogous way to similar analyses [29]. This background component is only included in the search for $B^+ \rightarrow D_s^+ \phi$ decays. The modes $\bar{B}_s^0 \rightarrow D_s^+ K^- K^{*0}$ and $\bar{B}_s^0 \rightarrow D_s^{*+} K^- K^{*0}$ form a background to $B^+ \rightarrow D_s^+ \phi$ decays when a low-momentum pion from the K^{*0} decay is not reconstructed. Additionally, a neutral pion or photon can be missed from the excited D_s^+ meson decay in the case of $\bar{B}_s^0 \rightarrow D_s^{*+} K^- K^{*0}$. The PDFs are determined from simulated events. The expected fractions in each category of the $B^+ \rightarrow D_s^+ \phi$ fit are fixed using simulated events. The decays $B_s^0 \rightarrow D_s^+ D_s^-$, $B_s^0 \rightarrow D_s^{*+} D_s^-$ and $B^0 \rightarrow D_s^+ D^-$ can form a background when a pion is not reconstructed from a D_s^+ or D^+ decaying to $K^+ K^- \pi^+$. The PDFs are also determined from simulated events, with the fractions in each $B^+ \rightarrow D_s^+ \phi$ fit category fixed. The result of the fit to $B^+ \rightarrow D_s^+ K^+ K^-$ candidates, including all the relevant background components is shown in Fig. 3. The result of the simultaneous fit to $B^+ \rightarrow D_s^+ \phi$ candidates in the different helicity angle and $m(K^+ K^-)$ mass categories is shown in Fig. 4. The three contributing D_s^+ meson decay modes are merged.

5 Systematic uncertainties

A number of different sources of systematic uncertainty are considered. The contribution from each source is detailed in Table 3.

Relative efficiencies: The calculation of the branching fractions requires a correction to the ratio of signal and normalisation yields to account for the difference in the selection efficiency of the two modes. All relative selection efficiencies except the PID and MVA efficiencies are determined from simulated events and the effect of having a limited simulation sample size is included as a systematic uncertainty. The relative efficiency for the PID and MVA requirements are determined from data control modes, including the samples of $B_s^0 \rightarrow J/\psi \phi$ and $\bar{B}_s^0 \rightarrow D_s^+ \pi^-$ decays used to test the MVA responses. Systematic uncertainties are assigned to account for the limited sizes of the control mode samples, kinematic differences between the control modes and the signal modes and differences between the data and simulation distributions that might affect the relative efficiency.

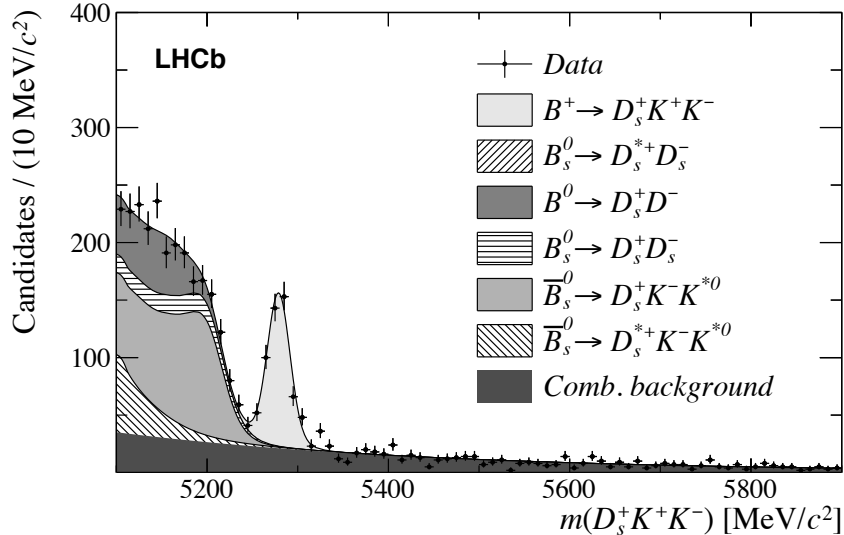


Figure 3: Mass distribution of $B^+ \rightarrow D_s^+ K^+ K^-$ candidates. The result of the fit to the data using the model described in Sec. 4.1 is overlaid, with the PDF components given in the legend.

Table 3: Systematic uncertainties contributing to the measurements of $\mathcal{B}(B^+ \rightarrow D_s^+ \phi)$ and $\mathcal{B}(B^+ \rightarrow D_s^+ K^+ K^-)$. The systematic uncertainty from the normalisation branching fraction is also included.

Source of uncertainty	$\mathcal{B}(B^+ \rightarrow D_s^+ \phi)$ ($\times 10^{-7}$)	$\mathcal{B}(B^+ \rightarrow D_s^+ K^+ K^-)$ ($\times 10^{-6}$)
Relative efficiencies	0.08	0.59
Signal and normalisation PDFs	0.04	0.04
Background PDFs	0.69	0.02
Charmless contribution	0.02	0.05
$B^+ \rightarrow D_s^+ K^+ K^-$ model	0.38	–
Normalisation	0.12	0.72

Signal and normalisation PDFs: Some parameters in the signal and normalisation PDFs are fixed to values obtained from simulation. These include the tail parameters, relative widths, and fractional amounts of the two CB functions that make up the PDFs. The values obtained from simulation have associated uncertainties arising from the limited simulation sample sizes. The nominal fits are repeated with the fixed parameters modified to values sampled from Gaussian distributions, with a width given by the parameter uncertainties. All parameters are changed simultaneously. For the fit to $B^+ \rightarrow D_s^+ \phi$ candidates, the fractions of events expected in each category of the fit are also included in the procedure. The resulting variation is assigned as the systematic uncertainty.

Background PDFs: Some of the PDFs for the background modes are taken directly from simulated events using one-dimensional kernel estimations [30]. In the nominal fit, these are smeared to account for the differences in the mass resolution between

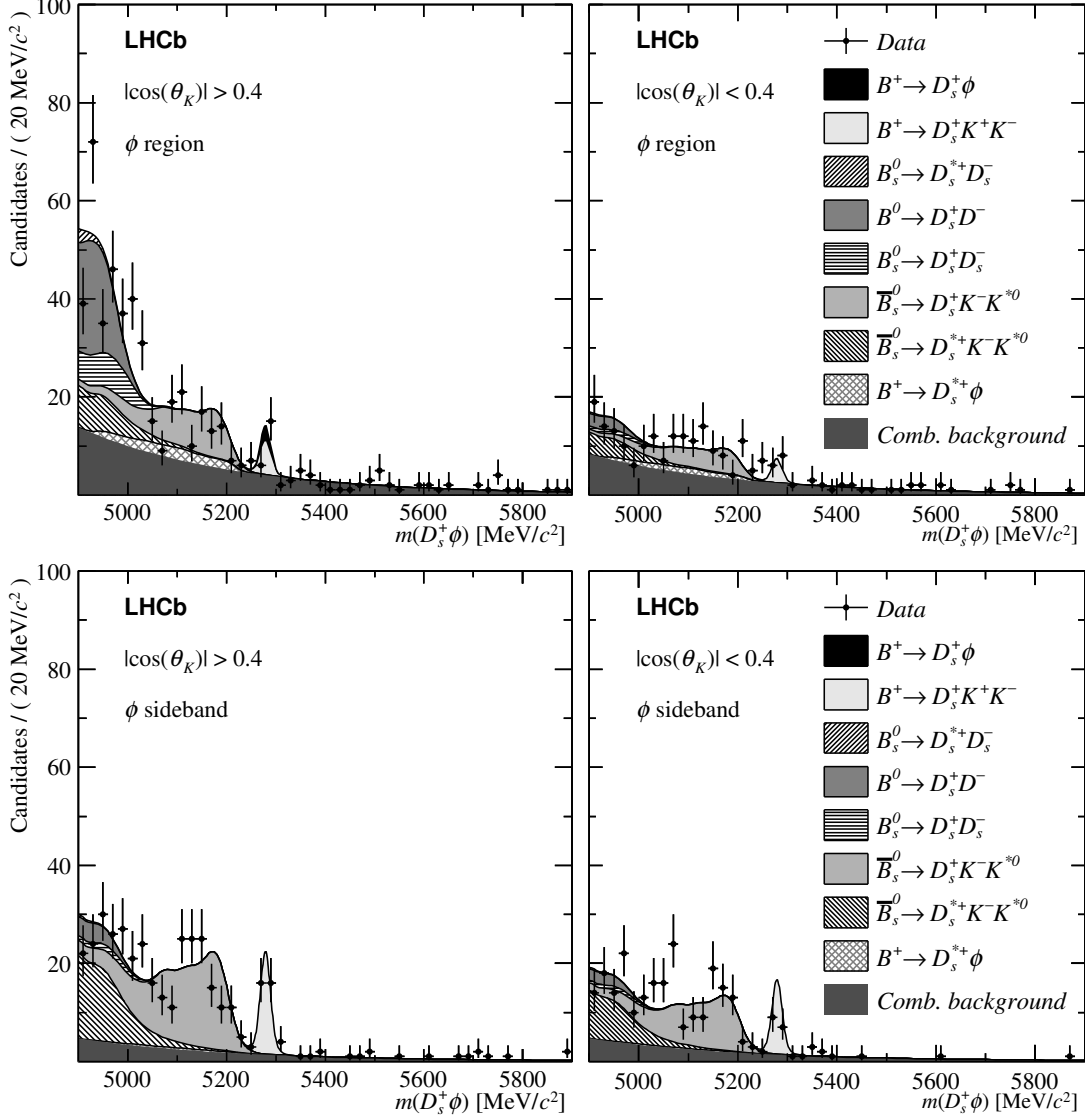


Figure 4: Mass distribution of $B^+ \rightarrow D_s^+ \phi$ candidates in (top) the ϕ mass region, and (bottom) the ϕ mass sideband. The plots on the left are in the helicity bin $|\cos \theta_K| > 0.4$ and the right are in $|\cos \theta_K| < 0.4$. The result of the fit to the data using the model described in Sec. 4.1 is overlaid, with the PDF components given in the legend. The $B^+ \rightarrow D_s^+ \phi$ decays (black) are expected to primarily contribute to the ϕ region with $|\cos \theta_K| > 0.4$.

data and simulation. To account for any systematic uncertainty arising from the choice of resolution difference, the fit is repeated, randomly varying the smearing resolution each time. The resulting variation in the branching fraction is assigned as a systematic uncertainty. Additionally, each partially reconstructed background PDF has fixed fractions in the different categories of the signal fit. To determine the effect on the branching fraction, these fractions are repeatedly sampled from Gaussian distributions with widths given by the statistical uncertainty on the fractions. For the combinatorial background shape, the choice of parametrisation is varied and the effect included in the systematic uncertainty.

Charmless contribution: Residual charmless and single-charm backgrounds are ex-

pected to remain in the final selection. These contributions are neglected in the calculation of the branching fractions. However, the shift in the branching fraction caused by numerically including the charmless yields is assigned as a systematic uncertainty.

$B^+ \rightarrow D_s^+ K^+ K^-$ model assumption: The fit to $B^+ \rightarrow D_s^+ \phi$ candidates includes a shape for $B^+ \rightarrow D_s^+ K^+ K^-$ decays that do not proceed via a ϕ meson. In order to distinguish this component from the signal, the different fractions of candidates in the four fit categories are exploited. This requires making assumptions as to which resonances contribute to the full $B^+ \rightarrow D_s^+ K^+ K^-$ decay model. The shape is assumed to be dominated by $f_0(980)$ and $a_0(980)$ resonances. Estimates of the uncertainties on the fractions are determined by considering the range in each fraction for the models considered. The variation in the branching fraction that results from varying these fractions within the uncertainties is assigned as the systematic uncertainty.

6 Results

6.1 Search for $B^+ \rightarrow D_s^+ K^+ K^-$ candidates

The fit to $B^+ \rightarrow D_s^+ K^+ K^-$ candidates finds a total yield of $N(B^+ \rightarrow D_s^+ K^+ K^-) = 443 \pm 29$ candidates. This constitutes the first observation of this decay mode. The branching fraction is calculated as

$$\mathcal{B}(B^+ \rightarrow D_s^+ K^+ K^-) = \frac{N_{\text{corr}}(B^+ \rightarrow D_s^+ K^+ K^-)}{N(B^+ \rightarrow D_s^+ \bar{D}^0)} \times \mathcal{B}(B^+ \rightarrow D_s^+ \bar{D}^0) \times \mathcal{B}(\bar{D}^0 \rightarrow K^+ K^-) \quad (2)$$

where $N(B^+ \rightarrow D_s^+ \bar{D}^0)$ is the yield of normalisation decays, and $N_{\text{corr}}(B^+ \rightarrow D_s^+ K^+ K^-)$ is defined to be

$$N_{\text{corr}}(B^+ \rightarrow D_s^+ K^+ K^-) = \sum_i \frac{W_i}{\epsilon_i^{\text{ratio}}}, \quad (3)$$

where W_i is the per-candidate weight, as determined by the *sPlot* technique for candidate i ; and $\epsilon_i^{\text{ratio}}$ represents the relative efficiency of the signal and normalisation modes $\epsilon_i(B^+ \rightarrow D_s^+ K^+ K^-) / \epsilon(B^+ \rightarrow D_s^+ \bar{D}^0)$ in the relevant bin of the $B^+ \rightarrow D_s^+ K^+ K^-$ Dalitz plot. The corrected yield ratio can be expressed as the ratio of signal and normalisation branching fractions using Eq. 2. The value is measured to be

$$\frac{N_{\text{corr}}(B^+ \rightarrow D_s^+ K^+ K^-)}{N(B^+ \rightarrow D_s^+ \bar{D}^0)} = \frac{\mathcal{B}(B^+ \rightarrow D_s^+ K^+ K^-)}{\mathcal{B}(B^+ \rightarrow D_s^+ \bar{D}^0) \mathcal{B}(\bar{D}^0 \rightarrow K^+ K^-)} = 0.197 \pm 0.015 \pm 0.017,$$

where the first uncertainty is statistical, and the second is systematic. The branching fraction for $B^+ \rightarrow D_s^+ K^+ K^-$ decays is determined to be

$$\mathcal{B}(B^+ \rightarrow D_s^+ K^+ K^-) = (7.1 \pm 0.5 \pm 0.6 \pm 0.7) \times 10^{-6},$$

where the first uncertainty is statistical, the second is systematic and the third from the branching fractions of $\bar{D}^0 \rightarrow K^+ K^-$ and of the normalisation mode $B^+ \rightarrow D_s^+ \bar{D}^0$. The values used for the branching fractions are $\mathcal{B}(D^0 \rightarrow K^+ K^-) = (4.01 \pm 0.07) \times 10^{-3}$ and

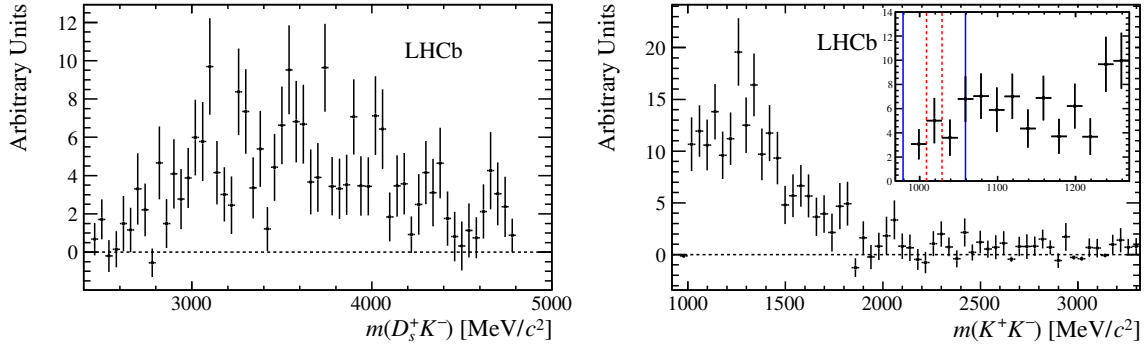


Figure 5: Projections of the background-subtracted two-body invariant masses (left) $m(D_s^+ K^-)$ and (right) $m(K^+ K^-)$ for $B^+ \rightarrow D_s^+ K^+ K^-$ decays. These plots are additionally weighted by a factor $1/\epsilon_i^{\text{ratio}}$ to correct for the efficiency variation across the phase space. An expansion of the ϕ region of $m(K^+ K^-)$ is inset where the same ϕ signal region and ϕ sideband region have been represented as in Fig. 2.

$\mathcal{B}(B^+ \rightarrow D_s^+ \bar{D}^0) = (9.0 \pm 0.9) \times 10^{-3}$ [11]. The two-body projections $m(D_s^+ K^-)$ and $m(K^+ K^-)$ are obtained for the signal component using the *sPlot* technique, shown in Fig. 5. No significant peak is observed in the ϕ region of the $m(K^+ K^-)$ plot; rather a broad distribution of candidates is found in the region up to $m(K^+ K^-) \simeq 1900 \text{ MeV}/c^2$.

6.2 Search for $B^+ \rightarrow D_s^+ \phi$ candidates

The fit to $B^+ \rightarrow D_s^+ \phi$ candidates finds a total yield of $N(B^+ \rightarrow D_s^+ \phi) = 5.3 \pm 6.7$, summed across all categories and D_s^+ meson decay modes. A yield of $N(B^+ \rightarrow D_s^+ K^- K^+) = 65 \pm 10$ is found, consistent with the yield obtained from the full $B^+ \rightarrow D_s^+ K^+ K^-$ measurement. The branching fraction for $B^+ \rightarrow D_s^+ \phi$ decays is calculated as

$$\mathcal{B}(B^+ \rightarrow D_s^+ \phi) = R \times \frac{\mathcal{B}(\bar{D}^0 \rightarrow K^+ K^-)}{\mathcal{B}(\phi \rightarrow K^+ K^-)} \times \mathcal{B}(B^+ \rightarrow D_s^+ \bar{D}^0), \quad (4)$$

where the branching fraction $\mathcal{B}(\phi \rightarrow K^+ K^-) = 0.489 \pm 0.005$ has been used [11].

The free variable R is defined to be the ratio of the signal and normalisation yields, corrected for the selection efficiencies. The yield of signal candidates in each D_s^+ mode is constructed from R and the normalisation yield for the given D_s^+ decay mode, $N(B^+ \rightarrow D_s^+ \bar{D}^0)$. The product of these two quantities is corrected by the ratio of selection efficiencies

$$N(B^+ \rightarrow D_s^+ \phi) = R \times N(B^+ \rightarrow D_s^+ \bar{D}^0) \times \frac{\epsilon(B^+ \rightarrow D_s^+ \phi)}{\epsilon(B^+ \rightarrow D_s^+ \bar{D}^0)}. \quad (5)$$

The simultaneous fit measures a single value of R for all D_s^+ decay mode categories. From an ensemble of pseudoexperiments, R is distributed normally. It can be written as the ratio of signal and normalisation branching fractions using Eq. 4. The value is determined to be

$$R = \frac{\mathcal{B}(B^+ \rightarrow D_s^+ \phi)}{\mathcal{B}(B^+ \rightarrow D_s^+ \bar{D}^0)} \times \frac{\mathcal{B}(\phi \rightarrow K^+ K^-)}{\mathcal{B}(\bar{D}^0 \rightarrow K^+ K^-)} = (1.6_{-1.9}^{+2.2} \pm 1.1) \times 10^{-3},$$

where the first uncertainty is statistical and the second systematic. This corresponds to a branching fraction for $B^+ \rightarrow D_s^+ \phi$ decays of

$$\mathcal{B}(B^+ \rightarrow D_s^+ \phi) = (1.2_{-1.4}^{+1.6} \pm 0.8 \pm 0.1) \times 10^{-7},$$

where the first uncertainty is statistical, the second systematic, and the third results from the uncertainty on the branching fractions $\mathcal{B}(B^+ \rightarrow D_s^+ \bar{D}^0)$, $\mathcal{B}(\phi \rightarrow K^+ K^-)$ and $\mathcal{B}(\bar{D}^0 \rightarrow K^+ K^-)$. Considering only the statistical uncertainty, the significance of the $B^+ \rightarrow D_s^+ \phi$ signal is 0.8 standard deviations (σ).

Upper limits at 95% and 90% confidence levels (CL) are determined using the Feldman-Cousins approach [31]. An ensemble of pseudoexperiments is generated for different values of the branching fraction $\mathcal{B}(B^+ \rightarrow D_s^+ \phi)$. These generated pseudoexperiments are then fitted with the nominal fit model to calculate the fitted branching fraction and associated statistical uncertainty, σ_{stat} . This method constructs confidence bands based on a likelihood ratio method, calculating the probability of fitting a branching fraction for a given generated branching fraction. This probability is assumed to follow a Gaussian distribution with width $\sigma = \sqrt{\sigma_{\text{stat}}^2 + \sigma_{\text{syst}}^2}$, where σ_{stat} and σ_{syst} are the statistical and systematic uncertainties. The dominant source of systematic uncertainty in this measurement is from the background PDFs. As the size of this uncertainty is not expected to vary as a function of the generated branching fraction, σ_{syst} is assumed to be constant. Nuisance parameters are accounted for using the plug-in method [32]. The generated confidence bands are shown in Fig. 6, where the statistical-only 90% CL and 95% CL bands are shown, along with the 95% CL band with systematic uncertainty included. This corresponds to a statistical-only 95% (90%) CL limit of $\mathcal{B}(B^+ \rightarrow D_s^+ \phi) < 4.4 \times 10^{-7}$ (3.9×10^{-7}), and a 95% (90%) CL limit including systematic uncertainties of

$$\mathcal{B}(B^+ \rightarrow D_s^+ \phi) < 4.9 \times 10^{-7} \quad (4.2 \times 10^{-7}).$$

7 Conclusions

A search for $B^+ \rightarrow D_s^+ K^+ K^-$ decays is performed. The branching fraction is determined to be

$$\mathcal{B}(B^+ \rightarrow D_s^+ K^+ K^-) = (7.1 \pm 0.5 \pm 0.6 \pm 0.7) \times 10^{-6},$$

where the first uncertainty is statistical, the second systematic and the third is due to the uncertainty on the branching fraction of the normalisation mode $B^+ \rightarrow D_s^+ \bar{D}^0$. This is the first observation of this decay mode. A search is also performed for the pure annihilation decay $B^+ \rightarrow D_s^+ \phi$, but no significant signal is observed and a limit of

$$\mathcal{B}(B^+ \rightarrow D_s^+ \phi) < 4.9 \times 10^{-7} \quad (4.2 \times 10^{-7})$$

is set on the branching fraction at 95% (90%) confidence level. The limit on $\mathcal{B}(B^+ \rightarrow D_s^+ \phi)$ presented here supersedes the previous result from LHCb [10].

This updated analysis benefits from the significantly larger data sample now available at LHCb to increase the reach of these searches. The previous measurement performed by LHCb reported evidence for the decay $B^+ \rightarrow D_s^+ \phi$ with a significance greater than 3σ .

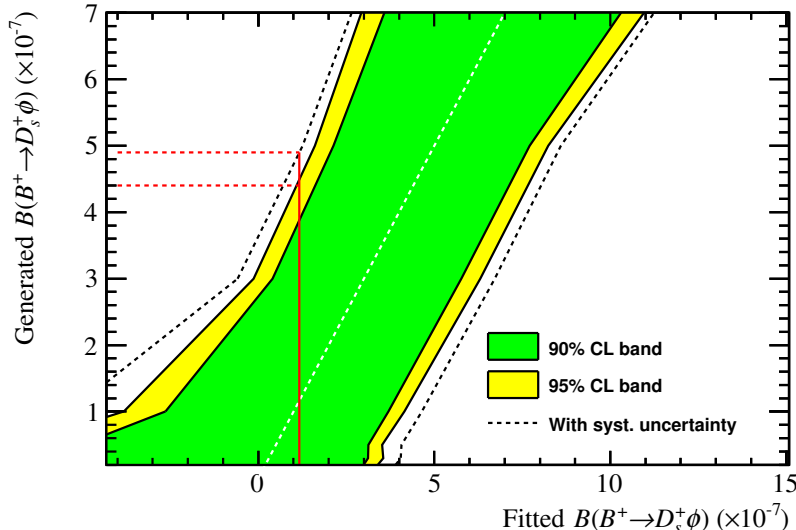


Figure 6: Confidence bands produced using the Feldman-Cousins approach. The green and yellow bands represent the statistical-only 90% and 95% CL bands. The black dotted line represents the 95% limit including systematic uncertainties. The measured value of the branching fraction is shown by the vertical red line, and the corresponding 95% CL limits, with and without systematic uncertainties, are represented by the dotted red lines.

This update determines that there is a sizeable contribution from $B^+ \rightarrow D_s^+ K^+ K^-$ decays that contribute within the ϕ -meson mass window that was previously not considered. The result is consistent with the prediction that rescattering contributions to $B^+ \rightarrow D_s^+ \phi$ decays are small.

Acknowledgements

We express our gratitude to our colleagues in the CERN accelerator departments for the excellent performance of the LHC. We thank the technical and administrative staff at the LHCb institutes. We acknowledge support from CERN and from the national agencies: CAPES, CNPq, FAPERJ and FINEP (Brazil); MOST and NSFC (China); CNRS/IN2P3 (France); BMBF, DFG and MPG (Germany); INFN (Italy); NWO (The Netherlands); MNiSW and NCN (Poland); MEN/IFA (Romania); MinES and FASO (Russia); MinECo (Spain); SNSF and SER (Switzerland); NASU (Ukraine); STFC (United Kingdom); NSF (USA). We acknowledge the computing resources that are provided by CERN, IN2P3 (France), KIT and DESY (Germany), INFN (Italy), SURF (The Netherlands), PIC (Spain), GridPP (United Kingdom), RRCKI and Yandex LLC (Russia), CSCS (Switzerland), IFIN-HH (Romania), CBPF (Brazil), PL-GRID (Poland) and OSC (USA). We are indebted to the communities behind the multiple open-source software packages on which we depend. Individual groups or members have received support from AvH Foundation (Germany), EPLANET, Marie Skłodowska-Curie Actions and ERC (European Union), ANR, Labex P2IO, ENIGMASS and OCEVU, and Région Auvergne-Rhône-Alpes (France), RFBR and Yandex LLC (Russia), GVA, XuntaGal and GENCAT (Spain), Herchel Smith Fund, the Royal Society, the English-Speaking Union and the Leverhulme Trust (United Kingdom).

References

- [1] BaBar collaboration, B. Aubert *et al.*, *Evidence for the rare decay $B^+ \rightarrow D_s^+ \pi^0$* , Phys. Rev. Lett. **98** (2007) 171801, [arXiv:hep-ex/0611030](#).
- [2] M. Gronau, D. London, and J. L. Rosner, *Rescattering contributions to rare B-meson decays*, Phys. Rev. **D87** (2013) 036008, [arXiv:1211.5785](#).
- [3] H. Zou, R.-H. Li, X.-X. Wang, and C.-D. Lu, *The CKM suppressed $B(B_s) \rightarrow \bar{D}_{(s)}P, \bar{D}_{(s)}V, \bar{D}_{(s)}^*P, \bar{D}_{(s)}^*V$ decays in perturbative QCD approach*, J. Phys. **G37** (2010) 015002, [arXiv:0908.1856](#).
- [4] R. Mohanta, *Searching for new physics in the rare decay $B^+ \rightarrow D_s^+ \phi$* , Phys. Lett. **B540** (2002) 241, [arXiv:hep-ph/0205297](#).
- [5] R. Mohanta and A. K. Giri, *Possible signatures of unparticles in rare annihilation type B decays*, Phys. Rev. **D76** (2007) 057701, [arXiv:0707.3308](#).
- [6] C.-D. Lu, *Calculation of pure annihilation type decay $B^+ \rightarrow D_s^+ \phi$* , Eur. Phys. J. **C24** (2002) 121, [arXiv:hep-ph/0112127](#).
- [7] HPQCD collaboration, R. J. Dowdall *et al.*, *B-meson decay constants from improved lattice nonrelativistic QCD and physical u, d, s and c quarks*, Phys. Rev. Lett. **110** (2013) 222003, [arXiv:1302.2644](#).
- [8] ETM collaboration, A. Bussone *et al.*, *Mass of the b quark and B-meson decay constants from $N_f = 2 + 1 + 1$ twisted-mass lattice QCD*, Phys. Rev. **D93** (2016) 114505, [arXiv:1603.04306](#).
- [9] Fermilab Lattice and MILC collaborations, A. Bazavov *et al.*, *$B_{(s)}^0$ -mixing matrix elements from lattice QCD for the Standard Model and beyond*, Phys. Rev. **D93** (2016) 113016, [arXiv:1602.03560](#).
- [10] LHCb collaboration, R. Aaij *et al.*, *First evidence for the annihilation decay mode $B^+ \rightarrow D_s^+ \phi$* , JHEP **02** (2013) 043, [arXiv:1210.1089](#).
- [11] Particle Data Group, C. Patrignani *et al.*, *Review of particle physics*, Chin. Phys. **C40** (2016) 100001.
- [12] LHCb collaboration, A. A. Alves Jr. *et al.*, *The LHCb detector at the LHC*, JINST **3** (2008) S08005.
- [13] LHCb collaboration, R. Aaij *et al.*, *LHCb detector performance*, Int. J. Mod. Phys. **A30** (2015) 1530022, [arXiv:1412.6352](#).
- [14] V. V. Gligorov and M. Williams, *Efficient, reliable and fast high-level triggering using a bonsai boosted decision tree*, JINST **8** (2013) P02013, [arXiv:1210.6861](#).
- [15] T. Sjöstrand, S. Mrenna, and P. Skands, *A brief introduction to PYTHIA 8.1*, Comput. Phys. Commun. **178** (2008) 852, [arXiv:0710.3820](#).

- [16] T. Sjöstrand, S. Mrenna, and P. Skands, *PYTHIA 6.4 physics and manual*, JHEP **05** (2006) 026, [arXiv:hep-ph/0603175](#).
- [17] I. Belyaev *et al.*, *Handling of the generation of primary events in Gauss, the LHCb simulation framework*, J. Phys. Conf. Ser. **331** (2011) 032047.
- [18] D. J. Lange, *The EvtGen particle decay simulation package*, Nucl. Instrum. Meth. **A462** (2001) 152.
- [19] P. Golonka and Z. Was, *PHOTOS Monte Carlo: A precision tool for QED corrections in Z and W decays*, Eur. Phys. J. **C45** (2006) 97, [arXiv:hep-ph/0506026](#).
- [20] Geant4 collaboration, J. Allison *et al.*, *Geant4 developments and applications*, IEEE Trans. Nucl. Sci. **53** (2006) 270; Geant4 collaboration, S. Agostinelli *et al.*, *Geant4: A simulation toolkit*, Nucl. Instrum. Meth. **A506** (2003) 250.
- [21] M. Clemencic *et al.*, *The LHCb simulation application, Gauss: Design, evolution and experience*, J. Phys. Conf. Ser. **331** (2011) 032023.
- [22] LHCb collaboration, R. Aaij *et al.*, *First observations of $\bar{B}_s^0 \rightarrow D^+ D^-$, $D_s^+ D^-$ and $D^0 \bar{D}^0$ decays*, Phys. Rev. **D87** (2013) 092007, [arXiv:1302.5854](#).
- [23] M. Pivk and F. R. Le Diberder, *sPlot: A statistical tool to unfold data distributions*, Nucl. Instrum. Meth. **A555** (2005) 356, [arXiv:physics/0402083](#).
- [24] L. Breiman, J. H. Friedman, R. A. Olshen, and C. J. Stone, *Classification and regression trees*, Wadsworth international group, Belmont, California, USA, 1984.
- [25] G. Punzi, *Sensitivity of searches for new signals and its optimization*, in *Statistical Problems in Particle Physics, Astrophysics, and Cosmology* (L. Lyons, R. Mount, and R. Reitmeyer, eds.), p. 79, 2003. [arXiv:physics/0308063](#).
- [26] W. D. Hulsbergen, *Decay chain fitting with a Kalman filter*, Nucl. Instrum. Meth. **A552** (2005) 566, [arXiv:physics/0503191](#).
- [27] T. Skwarnicki, *A study of the radiative cascade transitions between the Upsilon-prime and Upsilon resonances*, PhD thesis, Institute of Nuclear Physics, Krakow, 1986, DESY-F31-86-02.
- [28] LHCb collaboration, R. Aaij *et al.*, *Measurement of CP observables in $B^\pm \rightarrow D^{(*)} K^\pm$ and $B^\pm \rightarrow D^{(*)} \pi^\pm$ decays*, [arXiv:1708.06370](#), submitted to Phys. Lett. B.
- [29] LHCb collaboration, R. Aaij *et al.*, *Model-independent measurement of the CKM angle γ using $B^0 \rightarrow DK^{*0}$ decays with $D \rightarrow K_s^0 \pi^+ \pi^-$ and $K_s^0 K^+ K^-$* , JHEP **06** (2016) 131, [arXiv:1604.01525](#).
- [30] K. S. Cranmer, *Kernel estimation in high-energy physics*, Comput. Phys. Commun. **136** (2001) 198, [arXiv:hep-ex/0011057](#).
- [31] G. J. Feldman and R. D. Cousins, *A unified approach to the classical statistical analysis of small signals*, Phys. Rev. **D57** (1998) 3873, [arXiv:physics/9711021](#).

- [32] B. Sen, M. Walker, and M. Woodroffe, *On the unified method with nuisance parameters*, *Statistica Sinica* **19** (2009) 301.

LHCb collaboration

R. Aaij⁴⁰, B. Adeva³⁹, M. Adinolfi⁴⁸, Z. Ajaltouni⁵, S. Akar⁵⁹, J. Albrecht¹⁰, F. Alessio⁴⁰, M. Alexander⁵³, A. Alfonso Alberio³⁸, S. Ali⁴³, G. Alkhazov³¹, P. Alvarez Cartelle⁵⁵, A.A. Alves Jr⁵⁹, S. Amato², S. Amerio²³, Y. Amhis⁷, L. An³, L. Anderlini¹⁸, G. Andreassi⁴¹, M. Andreotti^{17,g}, J.E. Andrews⁶⁰, R.B. Appleby⁵⁶, F. Archilli⁴³, P. d'Argent¹², J. Arnau Romeu⁶, A. Artamonov³⁷, M. Artuso⁶¹, E. Aslanides⁶, M. Atzeni⁴², G. Auremma²⁶, M. Baalouch⁵, I. Babuschkin⁵⁶, S. Bachmann¹², J.J. Back⁵⁰, A. Badalov^{38,m}, C. Baesso⁶², S. Baker⁵⁵, V. Balagura^{7,b}, W. Baldini¹⁷, A. Baranov³⁵, R.J. Barlow⁵⁶, C. Barschel⁴⁰, S. Barsuk⁷, W. Barter⁵⁶, F. Baryshnikov³², V. Batozskaya²⁹, V. Battista⁴¹, A. Bay⁴¹, L. Beaucourt⁴, J. Beddow⁵³, F. Bedeschi²⁴, I. Bediaga¹, A. Beiter⁶¹, L.J. Bel⁴³, N. Belyi⁶³, V. Bellee⁴¹, N. Belloli^{21,i}, K. Belous³⁷, I. Belyaev^{32,40}, E. Ben-Haim⁸, G. Bencivenni¹⁹, S. Benson⁴³, S. Beranek⁹, A. Berezhnoy³³, R. Bernet⁴², D. Berninghoff¹², E. Bertholet⁸, A. Bertolin²³, C. Betancourt⁴², F. Betti¹⁵, M.-O. Bettler⁴⁰, M. van Beuzekom⁴³, I.a. Bezshyiko⁴², S. Bifani⁴⁷, P. Billoir⁸, A. Birnkraut¹⁰, A. Bizzeti^{18,u}, M. Bjørn⁵⁷, T. Blake⁵⁰, F. Blanc⁴¹, S. Blusk⁶¹, V. Bocci²⁶, T. Boettcher⁵⁸, A. Bondar^{36,w}, N. Bondar³¹, I. Bordyuzhin³², S. Borghi⁵⁶, M. Borisyak³⁵, M. Borsato³⁹, F. Bossu⁷, M. Boubdir⁹, T.J.V. Bowcock⁵⁴, E. Bowen⁴², C. Bozzi^{17,40}, S. Braun¹², T. Britton⁶¹, J. Brodzicka²⁷, D. Brundu¹⁶, E. Buchanan⁴⁸, C. Buri⁵⁶, A. Bursche^{16,f}, J. Buytaert⁴⁰, W. Byczynski⁴⁰, S. Cadeddu¹⁶, H. Cai⁶⁴, R. Calabrese^{17,g}, R. Calladine⁴⁷, M. Calvi^{21,i}, M. Calvo Gomez^{38,m}, A. Camboni^{38,m}, P. Campana¹⁹, D.H. Campora Perez⁴⁰, L. Capriotti⁵⁶, A. Carbone^{15,e}, G. Carboni^{25,j}, R. Cardinale^{20,h}, A. Cardini¹⁶, P. Carniti^{21,i}, L. Carson⁵², K. Carvalho Akiba², G. Casse⁵⁴, L. Cassina²¹, M. Cattaneo⁴⁰, G. Cavallero^{20,40,h}, R. Cenci^{24,t}, D. Chamont⁷, M.G. Chapman⁴⁸, M. Charles⁸, Ph. Charpentier⁴⁰, G. Chatzikonstantinidis⁴⁷, M. Chefdeville⁴, S. Chen¹⁶, S.F. Cheung⁵⁷, S.-G. Chitic⁴⁰, V. Chobanova^{39,40}, M. Chrzaszcz^{42,27}, A. Chubykin³¹, P. Ciambrone¹⁹, X. Cid Vidal³⁹, G. Ciezarek⁴³, P.E.L. Clarke⁵², M. Clemencic⁴⁰, H.V. Cliff⁴⁹, J. Closier⁴⁰, J. Cogan⁶, E. Cogneras⁵, V. Cogoni^{16,f}, L. Cojocariu³⁰, P. Collins⁴⁰, T. Colombo⁴⁰, A. Comerma-Montells¹², A. Contu⁴⁰, A. Cook⁴⁸, G. Coombs⁴⁰, S. Coquereau³⁸, G. Corti⁴⁰, M. Corvo^{17,g}, C.M. Costa Sobral⁵⁰, B. Couturier⁴⁰, G.A. Cowan⁵², D.C. Craik⁵⁸, A. Crocombe⁵⁰, M. Cruz Torres¹, R. Currie⁵², C. D'Ambrosio⁴⁰, F. Da Cunha Marinho², E. Dall'Occo⁴³, J. Dalseno⁴⁸, A. Davis³, O. De Aguiar Francisco⁴⁰, K. De Bruyn⁴⁰, S. De Capua⁵⁶, M. De Cian¹², J.M. De Miranda¹, L. De Paula², M. De Serio^{14,d}, P. De Simone¹⁹, C.T. Dean⁵³, D. Decamp⁴, L. Del Buono⁸, H.-P. Dembinski¹¹, M. Demmer¹⁰, A. Dendek²⁸, D. Derkach³⁵, O. Deschamps⁵, F. Dettori⁵⁴, B. Dey⁶⁵, A. Di Canto⁴⁰, P. Di Nezza¹⁹, H. Dijkstra⁴⁰, F. Dordei⁴⁰, M. Dorigo⁴⁰, A. Dosil Suárez³⁹, L. Douglas⁵³, A. Dovbnya⁴⁵, K. Dreimanis⁵⁴, L. Dufour⁴³, G. Dujany⁸, P. Durante⁴⁰, R. Dzhelezhyan³⁷, M. Dziewiecki¹², A. Dziurda⁴⁰, A. Dzyuba³¹, S. Easo⁵¹, M. Ebert⁵², U. Egede⁵⁵, V. Egorychev³², S. Eidelman^{36,w}, S. Eisenhardt⁵², U. Eitschberger¹⁰, R. Ekelhof¹⁰, L. Eklund⁵³, S. Ely⁶¹, S. Esen¹², H.M. Evans⁴⁹, T. Evans⁵⁷, A. Falabella¹⁵, N. Farley⁴⁷, S. Farry⁵⁴, D. Fazzini^{21,i}, L. Federici²⁵, D. Ferguson⁵², G. Fernandez³⁸, P. Fernandez Declara⁴⁰, A. Fernandez Prieto³⁹, F. Ferrari¹⁵, F. Ferreira Rodrigues², M. Ferro-Luzzi⁴⁰, S. Filippov³⁴, R.A. Fini¹⁴, M. Fiorini^{17,g}, M. Firlej²⁸, C. Fitzpatrick⁴¹, T. Fiutowski²⁸, F. Fleuret^{7,b}, K. Fohl⁴⁰, M. Fontana^{16,40}, F. Fontanelli^{20,h}, D.C. Forshaw⁶¹, R. Forty⁴⁰, V. Franco Lima⁵⁴, M. Frank⁴⁰, C. Frei⁴⁰, J. Fu^{22,q}, W. Funk⁴⁰, E. Furfaro^{25,j}, C. Färber⁴⁰, E. Gabriel⁵², A. Gallas Torreira³⁹, D. Galli^{15,e}, S. Gallorini²³, S. Gambetta⁵², M. Gandelman², P. Gandini²², Y. Gao³, L.M. Garcia Martin⁷⁰, J. García Pardiñas³⁹, J. Garra Tico⁴⁹, L. Garrido³⁸, P.J. Garsed⁴⁹, D. Gascon³⁸, C. Gaspar⁴⁰, L. Gavardi¹⁰, G. Gazzoni⁵, D. Gerick¹², E. Gersabeck⁵⁶, M. Gersabeck⁵⁶, T. Gershon⁵⁰, Ph. Ghez⁴, S. Giani⁴¹, V. Gibson⁴⁹, O.G. Girard⁴¹, L. Giubega³⁰, K. Gizdov⁵², V.V. Gligorov⁸, D. Golubkov³², A. Golutvin⁵⁵, A. Gomes^{1,a}, I.V. Gorelov³³, C. Gotti^{21,i}, E. Govorkova⁴³, J.P. Grabowski¹², R. Graciani Diaz³⁸,

L.A. Granado Cardoso⁴⁰, E. Graugés³⁸, E. Graverini⁴², G. Graziani¹⁸, A. Grecu³⁰, R. Greim⁹,
 P. Griffith¹⁶, L. Grillo²¹, L. Gruber⁴⁰, B.R. Gruberg Cazon⁵⁷, O. Grünberg⁶⁷, E. Gushchin³⁴,
 Yu. Guz³⁷, T. Gys⁴⁰, C. Göbel⁶², T. Hadavizadeh⁵⁷, C. Hadjivasiliou⁵, G. Haefeli⁴¹, C. Haen⁴⁰,
 S.C. Haines⁴⁹, B. Hamilton⁶⁰, X. Han¹², T.H. Hancock⁵⁷, S. Hansmann-Menzemer¹²,
 N. Harnew⁵⁷, S.T. Harnew⁴⁸, C. Hasse⁴⁰, M. Hatch⁴⁰, J. He⁶³, M. Hecker⁵⁵, K. Heinicke¹⁰,
 A. Heister⁹, K. Hennessy⁵⁴, P. Henrard⁵, L. Henry⁷⁰, E. van Herwijnen⁴⁰, M. Heß⁶⁷,
 A. Hicheur², D. Hill⁵⁷, C. Hombach⁵⁶, P.H. Hopchev⁴¹, W. Hu⁶⁵, Z.C. Huard⁵⁹,
 W. Hulsbergen⁴³, T. Humair⁵⁵, M. Hushchyn³⁵, D. Hutchcroft⁵⁴, P. Ibis¹⁰, M. Idzik²⁸, P. Ilten⁵⁸,
 R. Jacobsson⁴⁰, J. Jalocha⁵⁷, E. Jans⁴³, A. Jawahery⁶⁰, F. Jiang³, M. John⁵⁷, D. Johnson⁴⁰,
 C.R. Jones⁴⁹, C. Joram⁴⁰, B. Jost⁴⁰, N. Jurik⁵⁷, S. Kandybei⁴⁵, M. Karacson⁴⁰, J.M. Kariuki⁴⁸,
 S. Karodia⁵³, N. Kazeev³⁵, M. Kecke¹², F. Keizer⁴⁹, M. Kelsey⁶¹, M. Kenzie⁴⁹, T. Ketel⁴⁴,
 E. Khairullin³⁵, B. Khanji¹², C. Khurewathanakul⁴¹, T. Kirn⁹, S. Klaver⁵⁶, K. Klimaszewski²⁹,
 T. Klimkovich¹¹, S. Koliiev⁴⁶, M. Kolpin¹², R. Kopečna¹², P. Koppenburg⁴³, A. Kosmyntseva³²,
 S. Kotriakhova³¹, M. Kozeiha⁵, L. Kravchuk³⁴, M. Kreps⁵⁰, F. Kress⁵⁵, P. Krokovny^{36,w},
 F. Kruse¹⁰, W. Krzemien²⁹, W. Kucewicz^{27,l}, M. Kucharczyk²⁷, V. Kudryavtsev^{36,w},
 A.K. Kuonen⁴¹, T. Kvaratskheliya^{32,40}, D. Lacarrere⁴⁰, G. Lafferty⁵⁶, A. Lai¹⁶, G. Lanfranchi¹⁹,
 C. Langenbruch⁹, T. Latham⁵⁰, C. Lazzeroni⁴⁷, R. Le Gac⁶, A. Leflat^{33,40}, J. Lefrançois⁷,
 R. Lefèvre⁵, F. Lemaître⁴⁰, E. Lemos Cid³⁹, O. Leroy⁶, T. Lesiak²⁷, B. Leverington¹², P.-R. Li⁶³,
 T. Li³, Y. Li⁷, Z. Li⁶¹, T. Likhomanenko⁶⁸, R. Lindner⁴⁰, F. Lionetto⁴², V. Lisovskyi⁷, X. Liu³,
 D. Loh⁵⁰, A. Loi¹⁶, I. Longstaff⁵³, J.H. Lopes², D. Lucchesi^{23,o}, M. Lucio Martinez³⁹, H. Luo⁵²,
 A. Lupato²³, E. Luppi^{17,g}, O. Lupton⁴⁰, A. Lusiani²⁴, X. Lyu⁶³, F. Machefert⁷, F. Maciuc³⁰,
 V. Macko⁴¹, P. Mackowiak¹⁰, S. Maddrell-Mander⁴⁸, O. Maev^{31,40}, K. Maguire⁵⁶,
 D. Maisuzenko³¹, M.W. Majewski²⁸, S. Malde⁵⁷, B. Malecki²⁷, A. Malinin⁶⁸, T. Maltsev^{36,w},
 G. Manca^{16,f}, G. Mancinelli⁶, D. Marangotto^{22,q}, J. Maratas^{5,v}, J.F. Marchand⁴, U. Marconi¹⁵,
 C. Marin Benito³⁸, M. Marinangeli⁴¹, P. Marino⁴¹, J. Marks¹², G. Martellotti²⁶, M. Martin⁶,
 M. Martinelli⁴¹, D. Martinez Santos³⁹, F. Martinez Vidal⁷⁰, L.M. Massacrier⁷, A. Massafferri¹,
 R. Matev⁴⁰, A. Mathad⁵⁰, Z. Mathe⁴⁰, C. Matteuzzi²¹, A. Mauri⁴², E. Maurice^{7,b}, B. Maurin⁴¹,
 A. Mazurov⁴⁷, M. McCann^{55,40}, A. McNab⁵⁶, R. McNulty¹³, J.V. Mead⁵⁴, B. Meadows⁵⁹,
 C. Meaux⁶, F. Meier¹⁰, N. Meinert⁶⁷, D. Melnychuk²⁹, M. Merk⁴³, A. Merli^{22,40,q},
 E. Michielin²³, D.A. Milanese⁶⁶, E. Millard⁵⁰, M.-N. Minard⁴, L. Minzoni¹⁷, D.S. Mitzel¹²,
 A. Mogini⁸, J. Molina Rodriguez¹, T. Mombächer¹⁰, I.A. Monroy⁶⁶, S. Monteil⁵,
 M. Morandin²³, M.J. Morello^{24,t}, O. Morgunova⁶⁸, J. Moron²⁸, A.B. Morris⁵², R. Mountain⁶¹,
 F. Muheim⁵², M. Mulder⁴³, D. Müller⁵⁶, J. Müller¹⁰, K. Müller⁴², V. Müller¹⁰, P. Naik⁴⁸,
 T. Nakada⁴¹, R. Nandakumar⁵¹, A. Nandi⁵⁷, I. Nasteva², M. Needham⁵², N. Neri^{22,40},
 S. Neubert¹², N. Neufeld⁴⁰, M. Neuner¹², T.D. Nguyen⁴¹, C. Nguyen-Mau^{41,n}, S. Nieswand⁹,
 R. Niet¹⁰, N. Nikitin³³, T. Nikodem¹², A. Nogay⁶⁸, D.P. O’Hanlon⁵⁰, A. Oblakowska-Mucha²⁸,
 V. Obraztsov³⁷, S. Ogilvy¹⁹, R. Oldeman^{16,f}, C.J.G. Onderwater⁷¹, A. Ossowska²⁷,
 J.M. Otalora Goicochea², P. Owen⁴², A. Oyanguren⁷⁰, P.R. Pais⁴¹, A. Palano^{14,d},
 M. Palutan^{19,40}, A. Papanestis⁵¹, M. Pappagallo^{14,d}, L.L. Pappalardo^{17,g}, W. Parker⁶⁰,
 C. Parkes⁵⁶, G. Passaleva^{18,40}, A. Pastore^{14,d}, M. Patel⁵⁵, C. Patrignani^{15,e}, A. Pearce⁴⁰,
 A. Pellegrino⁴³, G. Penso²⁶, M. Pepe Altarelli⁴⁰, S. Perazzini⁴⁰, P. Perret⁵, L. Pescatore⁴¹,
 K. Petridis⁴⁸, A. Petrolini^{20,h}, A. Petrov⁶⁸, M. Petruzzo^{22,q}, E. Picatoste Olloqui³⁸,
 B. Pietrzyk⁴, M. Pikies²⁷, D. Pinci²⁶, F. Pisani⁴⁰, A. Pistone^{20,h}, A. Piucci¹², V. Placinta³⁰,
 S. Playfer⁵², M. Plo Casasus³⁹, F. Polci⁸, M. Poli Lener¹⁹, A. Poluektov⁵⁰, I. Polyakov⁶¹,
 E. Polcarpo², G.J. Pomery⁴⁸, S. Ponce⁴⁰, A. Popov³⁷, D. Popov^{11,40}, S. Poslavskii³⁷,
 C. Potterat², E. Price⁴⁸, J. Prisciandaro³⁹, C. Prouve⁴⁸, V. Pugatch⁴⁶, A. Puig Navarro⁴²,
 H. Pullen⁵⁷, G. Punzi^{24,p}, W. Qian⁵⁰, R. Quagliani^{7,48}, B. Quintana⁵, B. Rachwal²⁸,
 J.H. Rademacker⁴⁸, M. Rama²⁴, M. Ramos Pernas³⁹, M.S. Rangel², I. Raniuk^{45,†},
 F. Ratnikov³⁵, G. Raven⁴⁴, M. Ravonel Salzgeber⁴⁰, M. Reboud⁴, F. Redi⁵⁵, S. Reichert¹⁰,
 A.C. dos Reis¹, C. Remon Alepuz⁷⁰, V. Renaudin⁷, S. Ricciardi⁵¹, S. Richards⁴⁸, M. Rihl⁴⁰,

K. Rinnert⁵⁴, V. Rives Molina³⁸, P. Robbe⁷, A. Robert⁸, A.B. Rodrigues¹, E. Rodrigues⁵⁹, J.A. Rodriguez Lopez⁶⁶, A. Rogozhnikov³⁵, S. Roiser⁴⁰, A. Rollings⁵⁷, V. Romanovskiy³⁷, A. Romero Vidal³⁹, J.W. Ronayne¹³, M. Rotondo¹⁹, M.S. Rudolph⁶¹, T. Ruf⁴⁰, P. Ruiz Valls⁷⁰, J. Ruiz Vidal⁷⁰, J.J. Saborido Silva³⁹, E. Sadykhov³², N. Sagidova³¹, B. Saitta^{16,f}, V. Salustino Guimaraes⁶², C. Sanchez Mayordomo⁷⁰, B. Sanmartin Sedes³⁹, R. Santacesaria²⁶, C. Santamarina Rios³⁹, M. Santimaria¹⁹, E. Santovetti^{25,j}, G. Sarpis⁵⁶, A. Sarti^{19,k}, C. Satriano^{26,s}, A. Satta²⁵, D.M. Saunders⁴⁸, D. Savrina^{32,33}, S. Schael⁹, M. Schellenberg¹⁰, M. Schiller⁵³, H. Schindler⁴⁰, M. Schmelling¹¹, T. Schmelzer¹⁰, B. Schmidt⁴⁰, O. Schneider⁴¹, A. Schopper⁴⁰, H.F. Schreiner⁵⁹, M. Schubiger⁴¹, M.-H. Schune⁷, R. Schwemmer⁴⁰, B. Sciascia¹⁹, A. Sciubba^{26,k}, A. Semennikov³², E.S. Sepulveda⁸, A. Sergi⁴⁷, N. Serra⁴², J. Serrano⁶, L. Sestini²³, P. Seyfert⁴⁰, M. Shapkin³⁷, I. Shapoval⁴⁵, Y. Shcheglov³¹, T. Shears⁵⁴, L. Shekhtman^{36,w}, V. Shevchenko⁶⁸, B.G. Siddi¹⁷, R. Silva Coutinho⁴², L. Silva de Oliveira², G. Simi^{23,o}, S. Simone^{14,d}, M. Sirendi⁴⁹, N. Skidmore⁴⁸, T. Skwarnicki⁶¹, E. Smith⁵⁵, I.T. Smith⁵², J. Smith⁴⁹, M. Smith⁵⁵, I. Soares Lavra¹, M.D. Sokoloff⁵⁹, F.J.P. Soler⁵³, B. Souza De Paula², B. Spaan¹⁰, P. Spradlin⁵³, S. Sridharan⁴⁰, F. Stagni⁴⁰, M. Stahl¹², S. Stahl⁴⁰, P. Stefko⁴¹, S. Stefkova⁵⁵, O. Steinkamp⁴², S. Stemmler¹², O. Stenyakin³⁷, M. Stepanova³¹, H. Stevens¹⁰, S. Stone⁶¹, B. Storaci⁴², S. Stracka^{24,p}, M.E. Stramaglia⁴¹, M. Straticiuc³⁰, U. Straumann⁴², J. Sun³, L. Sun⁶⁴, W. Sutcliffe⁵⁵, K. Swientek²⁸, V. Syropoulos⁴⁴, T. Szumlak²⁸, M. Szymanski⁶³, S. T'Jampens⁴, A. Tayduganov⁶, T. Tekampe¹⁰, G. Tellarini^{17,g}, F. Teubert⁴⁰, E. Thomas⁴⁰, J. van Tilburg⁴³, M.J. Tilley⁵⁵, V. Tisserand⁴, M. Tobin⁴¹, S. Tolch⁴⁹, L. Tomassetti^{17,g}, D. Tonelli²⁴, F. Toriello⁶¹, R. Tourinho Jadallah Aoude¹, E. Tournefier⁴, M. Traill⁵³, M.T. Tran⁴¹, M. Tresch⁴², A. Trisovic⁴⁰, A. Tsaregorodtsev⁶, P. Tsopelas⁴³, A. Tully⁴⁹, N. Tuning^{43,40}, A. Ukleja²⁹, A. Usachov⁷, A. Ustyuzhanin³⁵, U. Uwer¹², C. Vacca^{16,f}, A. Vagner⁶⁹, V. Vagnoni^{15,40}, A. Valassi⁴⁰, S. Valat⁴⁰, G. Valenti¹⁵, R. Vazquez Gomez⁴⁰, P. Vazquez Regueiro³⁹, S. Vecchi¹⁷, M. van Veghel⁴³, J.J. Velthuis⁴⁸, M. Veltri^{18,r}, G. Veneziano⁵⁷, A. Venkateswaran⁶¹, T.A. Verlage⁹, M. Vernet⁵, M. Vesterinen⁵⁷, J.V. Viana Barbosa⁴⁰, B. Viaud⁷, D. Vieira⁶³, M. Vieites Diaz³⁹, H. Viemann⁶⁷, X. Vilasis-Cardona^{38,m}, M. Vitti⁴⁹, V. Volkov³³, A. Vollhardt⁴², B. Voneki⁴⁰, A. Vorobyev³¹, V. Vorobyev^{36,w}, C. Voß⁹, J.A. de Vries⁴³, C. Vázquez Sierra³⁹, R. Waldi⁶⁷, C. Wallace⁵⁰, R. Wallace¹³, J. Walsh²⁴, J. Wang⁶¹, D.R. Ward⁴⁹, H.M. Wark⁵⁴, N.K. Watson⁴⁷, D. Websdale⁵⁵, A. Weiden⁴², C. Weisser⁵⁸, M. Whitehead⁴⁰, J. Wicht⁵⁰, G. Wilkinson⁵⁷, M. Wilkinson⁶¹, M. Williams⁵⁶, M.P. Williams⁴⁷, M. Williams⁵⁸, T. Williams⁴⁷, F.F. Wilson^{51,40}, J. Wimberley⁶⁰, M. Winn⁷, J. Wishahi¹⁰, W. Wislicki²⁹, M. Witek²⁷, G. Wormser⁷, S.A. Wotton⁴⁹, K. Wraight⁵³, K. Wyllie⁴⁰, Y. Xie⁶⁵, M. Xu⁶⁵, Z. Xu⁴, Z. Yang³, Z. Yang⁶⁰, Y. Yao⁶¹, H. Yin⁶⁵, J. Yu⁶⁵, X. Yuan⁶¹, O. Yushchenko³⁷, K.A. Zarebski⁴⁷, M. Zavertyaev^{11,c}, L. Zhang³, Y. Zhang⁷, A. Zhelezov¹², Y. Zheng⁶³, X. Zhu³, V. Zhukov³³, J.B. Zonneveld⁵², S. Zucchelli¹⁵.

¹Centro Brasileiro de Pesquisas Físicas (CBPF), Rio de Janeiro, Brazil

²Universidade Federal do Rio de Janeiro (UFRJ), Rio de Janeiro, Brazil

³Center for High Energy Physics, Tsinghua University, Beijing, China

⁴LAPP, Université Savoie Mont-Blanc, CNRS/IN2P3, Annecy-Le-Vieux, France

⁵Clermont Université, Université Blaise Pascal, CNRS/IN2P3, LPC, Clermont-Ferrand, France

⁶Aix Marseille Univ, CNRS/IN2P3, CPPM, Marseille, France

⁷LAL, Univ. Paris-Sud, CNRS/IN2P3, Université Paris-Saclay, Orsay, France

⁸LPNHE, Université Pierre et Marie Curie, Université Paris Diderot, CNRS/IN2P3, Paris, France

⁹I. Physikalisches Institut, RWTH Aachen University, Aachen, Germany

¹⁰Fakultät Physik, Technische Universität Dortmund, Dortmund, Germany

¹¹Max-Planck-Institut für Kernphysik (MPIK), Heidelberg, Germany

¹²Physikalisches Institut, Ruprecht-Karls-Universität Heidelberg, Heidelberg, Germany

¹³School of Physics, University College Dublin, Dublin, Ireland

¹⁴Sezione INFN di Bari, Bari, Italy

- ¹⁵ *Sezione INFN di Bologna, Bologna, Italy*
- ¹⁶ *Sezione INFN di Cagliari, Cagliari, Italy*
- ¹⁷ *Universita e INFN, Ferrara, Ferrara, Italy*
- ¹⁸ *Sezione INFN di Firenze, Firenze, Italy*
- ¹⁹ *Laboratori Nazionali dell'INFN di Frascati, Frascati, Italy*
- ²⁰ *Sezione INFN di Genova, Genova, Italy*
- ²¹ *Universita e INFN, Milano-Bicocca, Milano, Italy*
- ²² *Sezione di Milano, Milano, Italy*
- ²³ *Sezione INFN di Padova, Padova, Italy*
- ²⁴ *Sezione INFN di Pisa, Pisa, Italy*
- ²⁵ *Sezione INFN di Roma Tor Vergata, Roma, Italy*
- ²⁶ *Sezione INFN di Roma La Sapienza, Roma, Italy*
- ²⁷ *Henryk Niewodniczanski Institute of Nuclear Physics Polish Academy of Sciences, Kraków, Poland*
- ²⁸ *AGH - University of Science and Technology, Faculty of Physics and Applied Computer Science, Kraków, Poland*
- ²⁹ *National Center for Nuclear Research (NCBJ), Warsaw, Poland*
- ³⁰ *Horia Hulubei National Institute of Physics and Nuclear Engineering, Bucharest-Magurele, Romania*
- ³¹ *Petersburg Nuclear Physics Institute (PNPI), Gatchina, Russia*
- ³² *Institute of Theoretical and Experimental Physics (ITEP), Moscow, Russia*
- ³³ *Institute of Nuclear Physics, Moscow State University (SINP MSU), Moscow, Russia*
- ³⁴ *Institute for Nuclear Research of the Russian Academy of Sciences (INR RAN), Moscow, Russia*
- ³⁵ *Yandex School of Data Analysis, Moscow, Russia*
- ³⁶ *Budker Institute of Nuclear Physics (SB RAS), Novosibirsk, Russia*
- ³⁷ *Institute for High Energy Physics (IHEP), Protvino, Russia*
- ³⁸ *ICCUB, Universitat de Barcelona, Barcelona, Spain*
- ³⁹ *Instituto Galego de Física de Altas Enerxías (IGFAE), Universidade de Santiago de Compostela, Santiago de Compostela, Spain*
- ⁴⁰ *European Organization for Nuclear Research (CERN), Geneva, Switzerland*
- ⁴¹ *Institute of Physics, Ecole Polytechnique Fédérale de Lausanne (EPFL), Lausanne, Switzerland*
- ⁴² *Physik-Institut, Universität Zürich, Zürich, Switzerland*
- ⁴³ *Nikhef National Institute for Subatomic Physics, Amsterdam, The Netherlands*
- ⁴⁴ *Nikhef National Institute for Subatomic Physics and VU University Amsterdam, Amsterdam, The Netherlands*
- ⁴⁵ *NSC Kharkiv Institute of Physics and Technology (NSC KIPT), Kharkiv, Ukraine*
- ⁴⁶ *Institute for Nuclear Research of the National Academy of Sciences (KINR), Kyiv, Ukraine*
- ⁴⁷ *University of Birmingham, Birmingham, United Kingdom*
- ⁴⁸ *H.H. Wills Physics Laboratory, University of Bristol, Bristol, United Kingdom*
- ⁴⁹ *Cavendish Laboratory, University of Cambridge, Cambridge, United Kingdom*
- ⁵⁰ *Department of Physics, University of Warwick, Coventry, United Kingdom*
- ⁵¹ *STFC Rutherford Appleton Laboratory, Didcot, United Kingdom*
- ⁵² *School of Physics and Astronomy, University of Edinburgh, Edinburgh, United Kingdom*
- ⁵³ *School of Physics and Astronomy, University of Glasgow, Glasgow, United Kingdom*
- ⁵⁴ *Oliver Lodge Laboratory, University of Liverpool, Liverpool, United Kingdom*
- ⁵⁵ *Imperial College London, London, United Kingdom*
- ⁵⁶ *School of Physics and Astronomy, University of Manchester, Manchester, United Kingdom*
- ⁵⁷ *Department of Physics, University of Oxford, Oxford, United Kingdom*
- ⁵⁸ *Massachusetts Institute of Technology, Cambridge, MA, United States*
- ⁵⁹ *University of Cincinnati, Cincinnati, OH, United States*
- ⁶⁰ *University of Maryland, College Park, MD, United States*
- ⁶¹ *Syracuse University, Syracuse, NY, United States*
- ⁶² *Pontifícia Universidade Católica do Rio de Janeiro (PUC-Rio), Rio de Janeiro, Brazil, associated to ²*
- ⁶³ *University of Chinese Academy of Sciences, Beijing, China, associated to ³*
- ⁶⁴ *School of Physics and Technology, Wuhan University, Wuhan, China, associated to ³*
- ⁶⁵ *Institute of Particle Physics, Central China Normal University, Wuhan, Hubei, China, associated to ³*
- ⁶⁶ *Departamento de Física, Universidad Nacional de Colombia, Bogota, Colombia, associated to ⁸*
- ⁶⁷ *Institut für Physik, Universität Rostock, Rostock, Germany, associated to ¹²*

- ⁶⁸ *National Research Centre Kurchatov Institute, Moscow, Russia, associated to* ³²
- ⁶⁹ *National Research Tomsk Polytechnic University, Tomsk, Russia, associated to* ³²
- ⁷⁰ *Instituto de Fisica Corpuscular, Centro Mixto Universidad de Valencia - CSIC, Valencia, Spain, associated to* ³⁸
- ⁷¹ *Van Swinderen Institute, University of Groningen, Groningen, The Netherlands, associated to* ⁴³
- ^a *Universidade Federal do Triângulo Mineiro (UFTM), Uberaba-MG, Brazil*
- ^b *Laboratoire Leprince-Ringuet, Palaiseau, France*
- ^c *P.N. Lebedev Physical Institute, Russian Academy of Science (LPI RAS), Moscow, Russia*
- ^d *Università di Bari, Bari, Italy*
- ^e *Università di Bologna, Bologna, Italy*
- ^f *Università di Cagliari, Cagliari, Italy*
- ^g *Università di Ferrara, Ferrara, Italy*
- ^h *Università di Genova, Genova, Italy*
- ⁱ *Università di Milano Bicocca, Milano, Italy*
- ^j *Università di Roma Tor Vergata, Roma, Italy*
- ^k *Università di Roma La Sapienza, Roma, Italy*
- ^l *AGH - University of Science and Technology, Faculty of Computer Science, Electronics and Telecommunications, Kraków, Poland*
- ^m *LIFAEELS, La Salle, Universitat Ramon Llull, Barcelona, Spain*
- ⁿ *Hanoi University of Science, Hanoi, Viet Nam*
- ^o *Università di Padova, Padova, Italy*
- ^p *Università di Pisa, Pisa, Italy*
- ^q *Università degli Studi di Milano, Milano, Italy*
- ^r *Università di Urbino, Urbino, Italy*
- ^s *Università della Basilicata, Potenza, Italy*
- ^t *Scuola Normale Superiore, Pisa, Italy*
- ^u *Università di Modena e Reggio Emilia, Modena, Italy*
- ^v *Iligan Institute of Technology (IIT), Iligan, Philippines*
- ^w *Novosibirsk State University, Novosibirsk, Russia*
- [†] *Deceased*